J Appl Electrochem (2009) 39:2369–2374
DOI 10.1007/s10800-009-9923-1

ORIGINAL PAPER

Characterization of $MgMn_xFe_{2-x}O_4$ as a possible cathode material for electrochemical reduction of NO_x

F. Bræstrup · K. K. Hansen

Received: 16 February 2009 / Accepted: 29 April 2009 / Published online: 26 May 2009
© Springer Science+Business Media B.V. 2009

Abstract *Spinel-type oxides of* $MgMn_xFe_{2-x}O_4$, $x = 0.0$, 0.2, 0.4, 0.6, 0.8, 1.0, were synthesized as a solid state reaction and characterized with dilatometry and resistivity measurements up to 1000 °C. Results showed a general decrease of the linear expansion and an increase in conductivity as a function of the Mn content. Point electrodes were analyzed from 300 to 600 °C in a pseudo-three-electrode setup in 1% NO, 1% NO_2, and 10% O_2 using cyclic voltammetry. The activities in O_2 were in general very low whereas the activities in NO were slightly higher. The activities in NO_2 were for all materials much higher than the activities in O_2. Even though Mn tends to decrease the activity of the materials, current ratios of I_{NO_x}/I_{O_2} have relatively high values in both NO and NO_2.

Keywords Spinel · Cone-electrodes · NO_x · O_2

1 Introduction

Spinel-type oxides (AB_2O_4, A = tetrahedral sites, B = octahedral sites) are in general poor electron conductors [1] and very bad oxygen ion conductors due to the almost perfect stoichiometric oxygen lattice [2]. Cations on the other hand tend to diffuse much easily through the structure [3]. Despite these properties spinel-type oxides are widely used in the industry because of their usefulness as magnetic materials, semi-conductors, pigments, catalysts, and refractories.

F. Bræstrup (✉) · K. K. Hansen
Fuel Cells and Solid State Chemistry Division, Risø National Laboratory for Sustainable Energy, Technical University of Denmark, Lyngby, Copenhagen, Denmark
e-mail: frantz.braestrup@risoe.dk

In search of a better fuel efficiency in the transportation sector, vehicles with a diesel-fired engine have increased their market share quite significantly over the years [4]. However, diesel-fired engines run with an excess of oxygen (lean conditions) which eliminates the use of the three-way converter which requires stoichiometric conditions to simultaneously catalyze oxidizing and reducing reactions. One of the main polluting agents from internal combustion processes in diesel- fired engines is the formation of NO_x (NO and NO_2) gases. So far the selective catalytic reduction process (SCR), where a reducing agent is injected into the exhaust gas upstream of the SCR catalyst, seems to be the only existing technology that can minimize the problem with NO_x gases from the diesel exhaust. However, SCR is most suitable for buses and trucks. But even in these cases there are problems with storage and escape of the reducing agent through the tailpipe of the vehicle. This shows that no perfect working technologies exist in this field [5].

Pancharatnam [6] suggested that NO_x could be removed over a solid state cell where NO_x gases are reduced at the cathode while O_2 is formed at the anode. However, since O_2 is also present in relatively high concentrations in the exhaust gas from a diesel-fired engine, it can also be reduced at the cathode which will lead to a high consumption of current. A good electrode material therefore has to be selective toward reduction of NO_x. Several attempts have been made to find cheap electrode materials of non-precious metals that can be used in such a cell. However, so far the materials, such as NiO, different perovskites, and individual members of the Ruddleston-Popper phases [7–11], have shown inadequate performance at the working conditions in a diesel-fired vehicle. The activity in O_2 is also in most cases too high compared to the activity in NO. RuO_2 [12] has also been suggested as possible electrode material; however, it is highly poisonous

and forms volatile of higher order oxides. Catalytic NO_x decomposition on spinel-type oxides [13–19] has been reported; however, to our knowledge only few observations on electrochemical decomposition on spinel-type electrode materials [20–22] have been presented in literature.

$MgFe_2O_4$ is a promising electrode material in NO and NO_2 sensors [22] and it has also received some interest as a possible humidity sensor material [23]. However, $MgFe_2O_4$ is a poor electronic conductor which will limit the current passing through the cell. The purpose of this article is therefore to investigate the effects of substituting Mn into the $MgFe_2O_4$ structure and to determine the conductivity with respect to the electro-catalytic activity. Since spinels act as isolators with respect to oxygen ion diffusion, it is most likely that in case of cell manufacturing, they have to be mixed with a solid state oxygen ion conductor. Therefore measurements on thermal expansion were also conducted on the different samples.

The spinel-type oxides were measured in a pseudo-three-electrode setup [24] suggested by Fabry et al. [25]. The advantage with this setup is that it suppresses the effect of geometry and morphology on the electrode behavior. Recorded data will therefore reflect the true electro-catalytic properties of the material. However, it is not possible to measure any gas conversion using a cone-shaped point electrode because of the small contact area. Instead, current ratios of I_{NO_x}/I_{O_2} are used as indicators of the apparent selectivity of the reduction of NO_x gases.

2 Experimental details

2.1 Sample preparation and X-ray diffraction

$MgMn_xFe_{2-x}O_4$, $x = 0.0, 0.2, 0.4, 0.6, 0.8, 1.0$, was synthesized as a solid state reaction using powder of metal oxides [MgO 99.99%, MnO_2 99.6%, and α-Fe_2O_3 99.9% (Alfa Aesar)]. The powder was mixed in an agate mortar and calcined at 900 °C for 30 h with a ramp rate of 120 °C/h. The powder was then crushed and the calcination process was repeated at 1050 °C. Relatively low sintering temperatures were used to avoid evaporation of Mn oxides. All samples were analyzed by X-ray diffraction using a STOE theta–theta diffractometer with a Cu anode. X-ray diffractograms were collected at $15° \leq 2\theta \leq 80°$ with a step width of 0.05°. Le Bail fits were carried out using the program Jana2000 [26] to determine the unit cell parameter *a*. Pseudo-Voigt profile functions were used, and the background was modeled with a 10 terms Legendre polynomials.

The powder was uniaxially pressed at 1 ton for 30 s into elongated bars and pellets which were placed in a rubber sleeve and pressed isostatically at 50 tons for 20 s. The samples were then calcined at 1100 °C for 10 h with a ramp rate of 50 °C/h. The elongated rods was cut into pieces of $4 \times 4 \times 18$ mm^3 and $4 \times 4 \times 12$ mm^3 to be used for resistivity and dilatometry measurements, respectively. The elongated pellets were mechanically tooled into identical cone-shaped electrodes, all having a diameter of 7.5 mm and with a cone side in an angle of 45° with the base.

2.2 Dilatometry

The linear thermal expansion was recorded using a NETZSCH DIL 402C dilatometer with a sample load of 30000 cN. Data were recorded in air with a flow rate of 50 mL/min. The samples were heated from room temperature up to 1000 °C and back at 2 °C/min. The sample remained at 1000 °C for 2 h. Data were calibrated to an Al_2O_3 standard at identical conditions.

2.3 Four-point DC resistivity measurement

The elongated bars ($4 \times 4 \times 18$ mm^3) were contacted with platinum leads and painted with Pt paste at each end of the bar. Two Pt potential probes with a fixed distance were positioned on one side of the bar. The data collection was made with an in-house data acquisition software, ELCHEMEA. The resistivity was measured every 5 min from room temperature to 1000 °C and back again with a 2-h dwell at every 50 °C interval and using a ramp rate of 2 °C/min. The porosity of the samples were measured with a Micromeritics AutoPore IV Mercury Porosimeter to correct the resistivities using Bruggeman formula [27].

2.4 Cyclic voltammetry and impedance spectroscopy

Cyclic voltammetry and impedance spectroscopy were recorded with a Gamry Femtostate in a pseudo-three-electrode setup on the cone-shaped electrodes. The base of the cone was painted with Au paste which acted as current collector. The cone, acting as the working electrode, was arranged with the tip placed downward on a polished one-end closed YSZ-tube (Yttrium-stabilized Zirconia) electrolyte containing air as reference gas. The thickness of the electrolyte was approximately 2 mm. The inside of the tube was painted with Ag paste and fired at 600 °C to get a good electrical contact. The Ag electrode was then used as the counter/reference electrode. The much smaller contact area of the cone electrode (point electrode), compared to the counter electrode, suppressed a polarization of the counter electrode as it was at the same time constantly exposed to a reference gas. A reference electrode could therefore be placed together with the counter electrode (a pseudo-three-electrode setup).

Data were recorded in 10% O_2 in Ar, 1% NO in Ar (Air Liquide) at 300, 400, 500, and 600 °C, and in 1% NO_2 in Ar (Air Liquide) at 300 and 400 °C. A flow rate of 20 mL/min was applied during all measurements. A 1 h equilibrium time was used to record the open circuit voltage (OCV) before recording the voltammograms in the potential range of −0.6 to 0.6 V with different sweep rates (1.0 and 10 mVs^{-1}). In order to compare the different electrode materials directly, the recorded current was converted into current densities by dividing with the contact area between the electrode and the electrolyte. The contact area was determined by using Newman's formula [28], Eq. 1,

$$r = \frac{1}{4\sigma R_e}, \tag{1}$$

where r is the radius of the circular contact area, σ is the specific conductivity of the electrolyte material, and R_e is the electrolyte resistance. σ can be determined from Eq. 2 [29].

$$\sigma = \frac{1.51 \cdot 10^6}{T} \cdot e^{\frac{-90.7[\mathrm{kJmol}^{-1}]}{RT}}, \tag{2}$$

where T and R are the temperature and the gas constant, respectively. R_e (see Table 1) was determined with impedance spectroscopy recorded from 177793(1) to 0.050(1) Hz with 10 points/decade and an amplitude of 24 mV (rms). Uncertainties on the contact areas were less than 10%. No corrections were made for the *IR* drop since calculations showed that the corrections were less than 1% at all temperatures.

3 Results and discussions

3.1 X-ray diffraction

All samples were analyzed as single phase cubic spinel-type oxides. Plotting the unit cell parameter a as a function of the Mn content shows that a only changes a little when Fe is substituted by Mn. Mg^{2+} ions have a strong preference to occupy the B sites and partially occupy the A sites [30]. Fe^{3+} on the other hand occupies both A and B sites with no preference, since their ionic radii are very similar [31]. Mn^{3+} tends to occupy B sites instead of A sites [32]. However, the ionic radius of Mn^{3+} is slightly bigger than that of Fe^{3+},[1] which will explain the small increase of the unit cell as more Mn is incorporated into the structure. Earlier reports [33] show similar increase in unit cell, but they state that the Mn content could not exceed $x = 0.4$ in order to synthesize a single phase powder. However, magnetic measurements on [34] $MgMn_xFe_{2-x}O_4, x \geq 1$ show that the material could be synthesized as a single phase with a solid state reaction (Fig. 1).

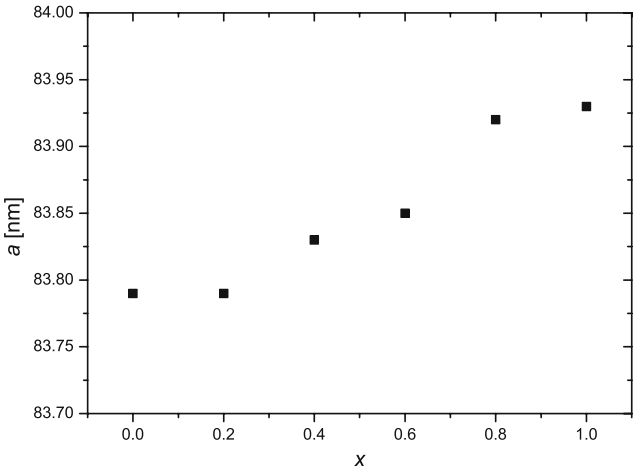

Fig. 1 Unit cell parameters, a, measured at different spinel compositions. A small increase in a is observed. x refers to the Mn content. Error bars are at the same magnitude as the dimension of the points

Table 1 Electrode porosities, Curie temperatures, T_c, expansion coefficients, α, and mean values of the electrolyte resistance, $\langle R_e \rangle$

Compound	Porosities (%)	T_c (°C)	α (°C^{-1})	$\langle R_e \rangle$ (MΩ)
$MgFe_2O_4$	27.18	322	$1.25(1) \cdot 10^{-5}$	2.5(2)
$MgMn_{0.2}Fe_{1.8}O_4$	29.92	304	$1.40(1) \cdot 10^{-5}$	7.4(3)
$MgMn_{0.4}Fe_{1.6}O_4$	33.16	251	$1.27(1) \cdot 10^{-5}$	12(4)
$MgMn_{0.6}Fe_{1.4}O_4$	33.78	163	$1.195(5) \cdot 10^{-5}$	7.1(2)
$MgMn_{0.8}Fe_{1.2}O_4$	37.92	141	$1.05(1) \cdot 10^{-5}$	13(3)
$MgMnFeO_4$	32.04	138	$1.010(9) \cdot 10^{-5}$	4.7(4)

The expansion coefficients are mean values calculated from 600 to 800 °C

3.2 Dilatometry and resistivity measurements

Figure 2 shows the dilatometry measurements of the samples. It shows, with the exception of $MgFe_2O_4$, a gradual decrease of the linear thermal expansion as more Mn is incorporated into the structure. The graphs (not shown for all materials) of the expansion coefficient show for all samples a peak positioned around 150−325 °C. The shape and position of the peaks agrees with the expected Curie temperature, T_c [35–37]. Figure 3 shows an example of the thermal expansion and expansion coefficient in the case of $MgMn_{0.2}Fe_{1.8}O_4$. Table 1 shows the decreasing Curie temperatures and the mean expansion coefficient in the temperature range of 600 to 800 °C. As discussed in the Introduction, spinels are in general bad oxygen ion

[1] http://www.webelements.com.

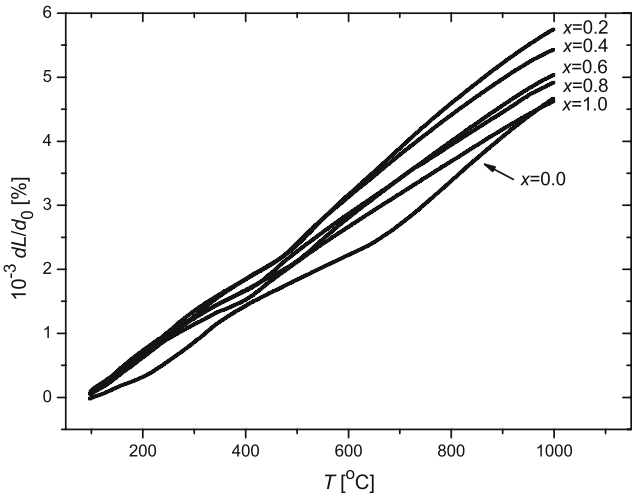

Fig. 2 Linear expansion of the different electrode materials measured in the temperature range of 80 to 1000 °C. *x* refers to the Mn content

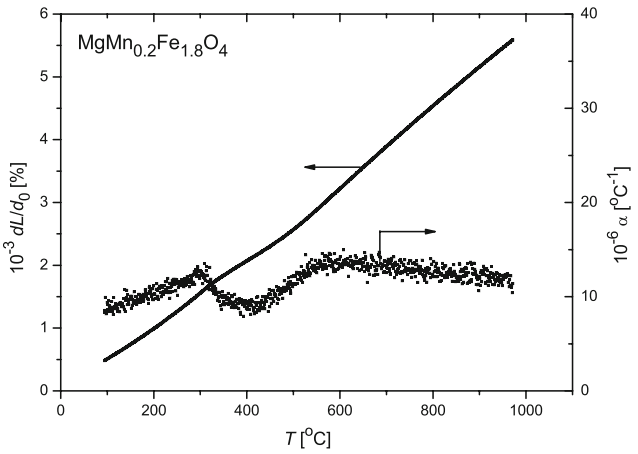

Fig. 3 Linear expansion and the expansion coefficient recorded on the $MgMn_{0.2}Fe_{1.8}O_4$ electrode. The Curie temperature can easily be detected at ~304 °C

conductors. Therefore, an oxygen ion material, such as $Ce_{0.9}Gd_{0.1}O_{1.95}$ (CGO10), must be mixed with the spinel material when more advanced cells need to be produced. Results show that the thermal expansion coefficient of the spinels is in general smaller than the thermal expansion coefficient of CGO10 ($\alpha = 11.9 \cdot 10^{-6}$ °C^{-1}); however, it should be possible to manufacture a suitable microstructure based on similar expansion coefficients in solid oxide fuel cells [38, 39]. Experiments however must be made to verify this.

Figure 4 shows the resistivities of the samples converted into Bruggeman-corrected specific conductivities. Results show that the conductivity increases when Fe is substituted with Mn. The conductivity is mainly caused by exchange interaction between B sites ($B-O^{2-}-B$) with hopping of localized *d*-electrons between cations [40, 41]. Substituting

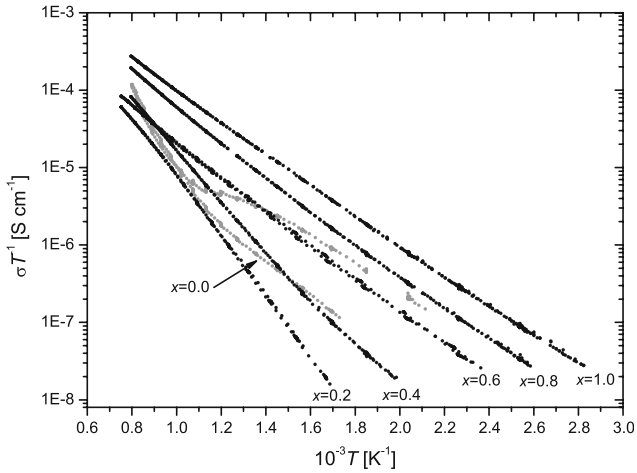

Fig. 4 Four-point DC conductivity measurements of the spinels measured from room temperature to 1000 °C in air. *x* refers to the Mn content

Mn into the structure will increase the conductivity as Mn can exist in more than one valence state (2+, 3+, and 4+) with Mn^{2+} primarily occupying the A sites and Mn^{3+} and Mn^{4+} occupying the B sites [32]. It is however believed that the oxidation state on Mn found in the samples is primarily 3+.

3.3 Cyclic voltammetry

The activity in 10% O_2 is for all materials very low ($\ll$1 mA cm^{-2}, −0.6 V), and within the uncertainties of the recorded data and contact areas (10%) it was not possible to determine a general trend with respect to activities and the Mn content.

The cathodic activities recorded in 1% NO at 400, 500 and 600 °C are low, and therefore, differences between the Mn-containing materials are small. Therefore only the results for some of the electrodes are shown in the figures. $MgMn_{0.4}Fe_{1.6}O_4$ has a slightly higher cathodic activity (−0.6 V) at 400 and 500 °C than the other Mn-containing samples. At all temperatures, the cathodic activity on $MgFe_2O_4$ was significantly higher (see Fig. 5). It is not known why $MgMn_{0.4}Fe_{1.6}O_4$ has higher activities but porosity measurements show no distinct differences compared to the other electrodes.

Data recorded in 1% NO_2 show a higher activity of the electrodes compared with the recorded data in NO and O_2. Earlier reports show similar trend on ferrite spinel-type electrodes [22, 42] and perovskites [8]. However, the cathodic activities of the Mn-containing electrodes are significantly lower compared to those of $MgFe_2O_4$ as also observed in NO. The activity of $MgMn_{0.2}Fe_{1.8}O_4$ is slightly higher than that of the other electrodes at 400 °C, whereas $MgMn_{0.8}Fe_{1.2}O_4$ shows higher activity at 300 °C (not shown) (Fig. 6).

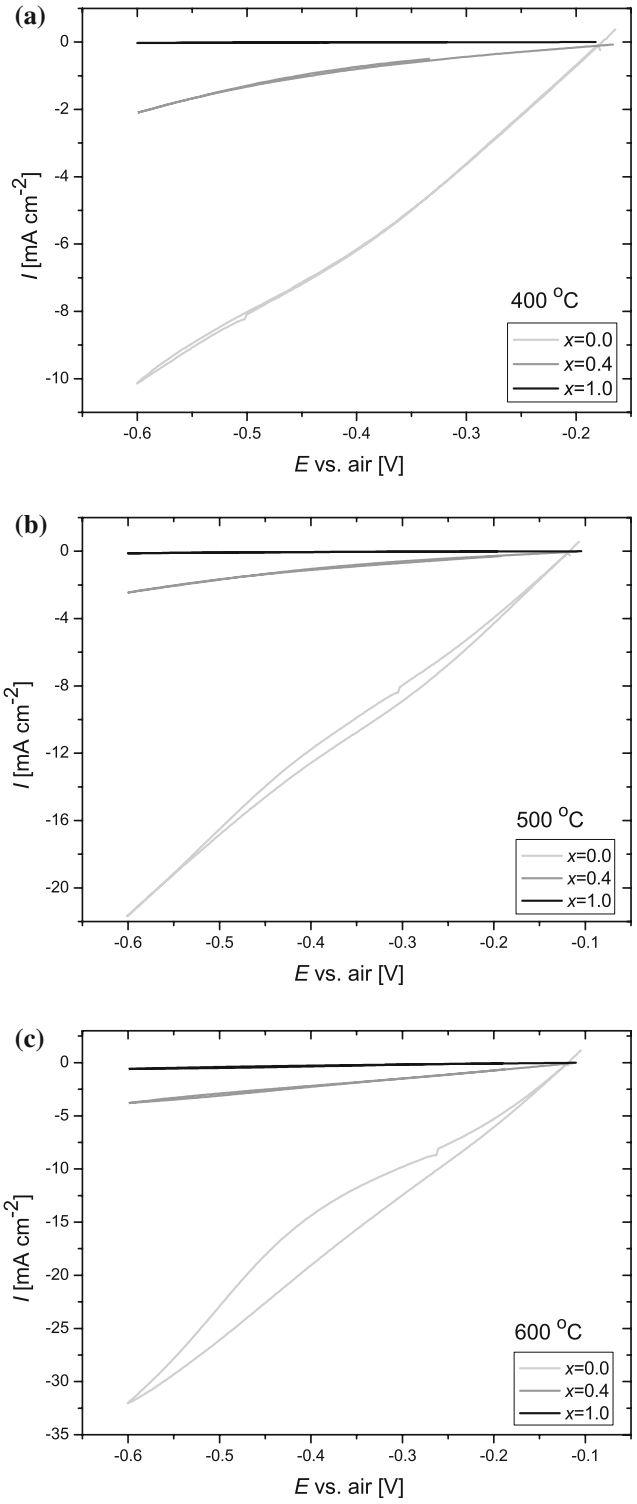

Fig. 5 Cyclic voltammograms on $MgMn_xFe_{2-x}O_4$. (**a**), (**b**), and (**c**) show a part of the voltammograms recorded at 400, 500, and 600 °C, respectively. The voltammograms were recorded in 1% NO with air as reference gas (sweep rate: 1 mVs^{-1}). Voltammograms recorded at 10 mVs^{-1} looked similar

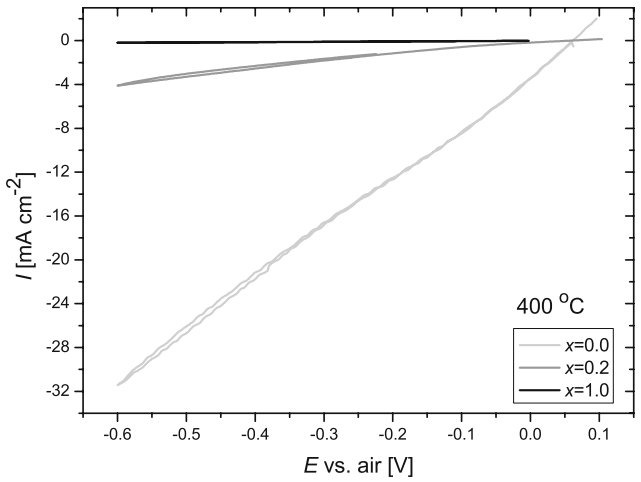

Fig. 6 Part of the cyclic voltammograms recorded at 400 °C in 1% NO_2 with a sweep rate of 1 mVs^{-1}. Voltammograms recorded at 10 mVs^{-1} looked similar

As previously discussed (see Introduction), current ratios of I_{NO_x}/I_{O_2} can be used as a tool to evaluate the electrode materials. Figure 7 shows the current ratios of I_{NO}/I_{O_2} and I_{NO_2}/I_{O_2} . At 400 °C, current ratios of I_{NO_2}/I_{O_2} show ratios of 25−30, with the exception of $MgMn_{0.4}Fe_{1.6}O_4$ which has a much higher current ratio of ∼65. Measurements were repeated with the same result, so it was not possible to explain the one-point jump on the curve. At 300 °C, current ratios increase with $MgFe_2O_4$ having the highest value of ∼135. It then drops to 40−50 for the Mn-containing electrodes.

Current ratios of I_{NO}/I_{O_2}. show in general much lower values compared to I_{NO_2}/I_{O_2}. At 600 °C current ratios are low and in the range of 1 to 3. At 500 °C, the highest current ratio is observed for $MgFe_2O_4$; however, the curves show a small broad peak at $0.4 \leq x \leq 0.6$. Still ratios only range from 1 to 5 for the Mn-containing electrodes. At 400 °C we see a large peak at $0.2 \leq x \leq 0.8$ with a maximum current ratio of ∼46. We were not able to explain the sudden drop at $x = 0.2$, and again porosity measurements did not help answer it either. We therefore believe that the porosity of the electrode materials have very little effect on the recorded data from a cone setup.

4 Conclusion

We have successfully synthesized single phase spinel-type oxides with a composition of $MgMn_xFe_{2-x}O_4$, $x = 0.0, 0.2,$

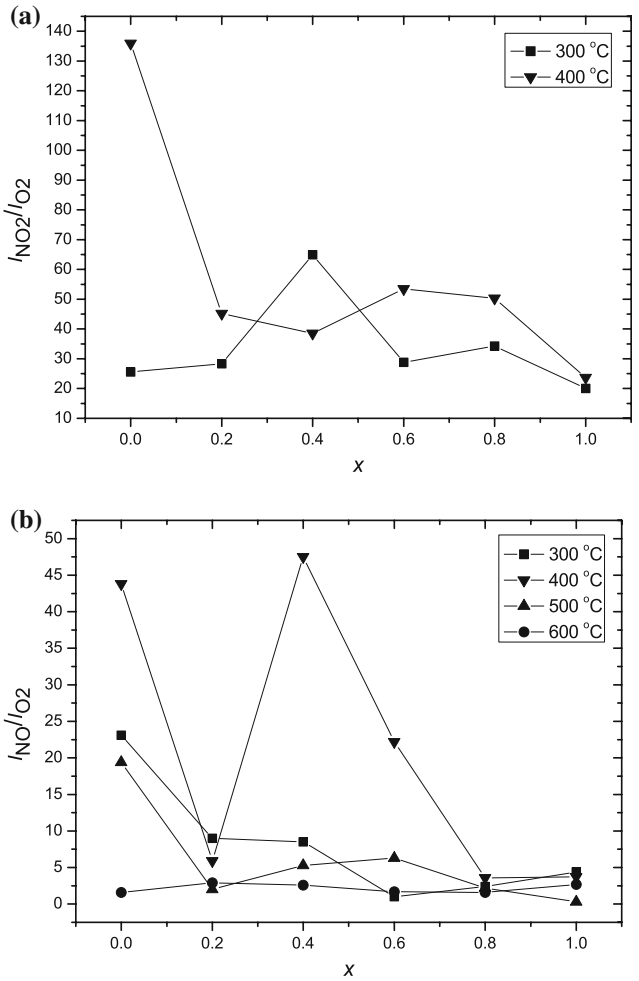

Fig. 7 Current ratios of (**a**) I_{NO_2}/I_{O_2}. and (**b**) I_{NO}/I_{O2} recorded on $MgMn_xFe_{2-x}O_4$ with an applied potential of −0.6 V. *x* refers to the Mn content

0.4, 0.6, 0.8, 1.0, using the solid state reactions. Dilatometry measurements showed a decreasing linear thermal expansion for the Mn-containing materials. Conductivity measurements show an increase in the electric conductivity when more Mn is incorporated into the structure. Data recorded with cyclic voltammetry in 1% NO, 1% NO_2 and 10% O_2 showed a decreasing activity when Mn was incorporated into the structure; however, current ratios are still relatively high compared to those of $MgFe_2O_4$.

Acknowledgments The Danish Council for Strategic Research (project no: 2194-05-0067) is thanked for the financial support. We would also like to thank the colleagues of the Fuel Cells and Solid State Chemistry Division for fruitful discussions.

References

1. Petric A, Ling H (2007) J Am Ceram Soc 90:1515
2. O'Bryan HM, DiMarcello FV (1970) J Am Ceram Soc 53:413
3. Dieckmann R (1984) Solid State Ionics 12:1
4. Seguin C (2006) Diesel car sales set to overtake petrol in Europe. http://www.pwc.com
5. http://www.dieselNet.com/news/2007/02delphi.php, Delpi announces ammonia sensor for SCR systems
6. Pancharatnam S, Huggins RA, Mason DM (1975) J Electrochem Soc 122:869
7. Simonsen VLE, Johnsen MM, Hansen KK (2007) Top Catal 45:131
8. Hansen KK (2007) Electrochem Commun 9:2721
9. Hansen KK, Skou EM, Christensen H (2000) J Electrochem Soc 147:2007
10. Hansen KK, Skou EM, Christensen H (2005) Solid State Ionics 176:915
11. Simonsen VLE, Nørskov L, Hansen KK (2008) J Solid State Electrochem 12:1573
12. Iwayama K, Wang X (1998) Appl Catal B 19:137
13. Shangguan WF, Teraoka Y, Kagawa S (1996) Appl Catal B 8:217
14. Shangguan WF, Teraoka Y, Kagawa S (1997) Appl Catal B 12:237
15. Shangguan WF, Teraoka Y, Kagawa S (1998) Appl Catal B 16:149
16. Haneda M, Kintaichi Y, Hamada H (2005) Appl Catal B 55:169–175
17. Drouet C, Alphonse P, Rousset A (2001) Appl Catal B 33:35
18. Chen L, Horiuchi T, Mori T (1999) Catal Lett 60:237
19. Fino D, Russo N, Saracco G, Specchia V (2006) J Catal 242:38
20. Simonsen VLE, Find D, Lilliedal M, Petersen R, Hansen KK, (2007) Top Catal 45:143
21. Hansen KK, Christensen H, Skou EM (2000) Ionics 6:340
22. Bræstrup F, Hansen KK (2008) The $NiFe_2O_4$–$MgFe_2O_4$ series as electrode materials for electrochemical reduction of NO_x. J Solid State Electrochem. doi:10.1007/s1000800806539
23. Gusmano G (1993) J Mater Sci 28:6195
24. Hansen KK, Christensen H, Skou EM, Skaarup SV (2000) J Appl Electrochem 30:193
25. Fabry P, Kleitz M, Deportes C (1972) J Solid State Chem 5:1
26. Petříček V, Dusek M, Palatinus L (2000) Jana2000. The crystallographic computing system. Institute of Physics, Praha, Czech Republic
27. Bruggeman DAG (1935) Ann Phys 24:636
28. Newman J (1966) J Electrochem Soc 113:501
29. Singhal SC, Dokiya M (2003) In Proceedings of the solid oxide fuel cells VIII, vol 7. Electrochem Soc Inc., New York, p 400
30. Kulkarni R, Joshi H (1985) Solid State Commun 53:1005
31. Klein C, Hurlbut CS, Dana JD (1998) Manual of mineralogy, 21st edn. Wiley, New York
32. Gillot B, Baudour JL, Bouree F, Metz R, Legros R, Rousset A (1992) Solid State Ionics 58:155
33. Hirota K, Saruwatari K, Kato M, Nakade K (2008) Sci Eng Rev Doshisha Univ 49:1
34. Zhang CL, Yeo S, Horibe Y, Choi YJ, Guha S, Croft M, Cheong SW (2007) Appl Phys Lett 90:133123
35. Touloukian YS, Ho CY (1977) Thermophysical properties of matter. The TPRC data series, vol 13. Plenum Pub Co., New York
36. Harrison RJ, Putnis A (1999) Phys Chem Mineral 26:322
37. Turkin AI, Drebushchak VA (2004) J Cryst Growth 265:165
38. Corbel G, Mestiri S, Lacorre P (2005) Solid State Sci 7:1216
39. Mori M, Hiei Y, Sammes NM, Tompsett GA (2000) J Electrochem Soc 147:1295
40. Ata-Allah SS, Fayek MK, Yehia M (2004) J Magn Magn Mater 279:411
41. Ata-Allah SS, Sayedamed FM, Kaiser M, Hashhash AM (2005) J Mater Sci 40:2923
42. Bræstrup F, Hansen KK (2009) $NiCr_xFe_{2-x}O_4$ as cathode materials for electrochemical reduction of NO_x. J Solid State Electrochem. doi:10.1007/s10008-009-0801-x